

Extreme compound events in the equatorial and South Atlantic

Received: 5 August 2024

Accepted: 17 March 2025

Published online: 16 April 2025



Regina R. Rodrigues¹✉, Camila Artana², Afonso Gonçalves Neto¹, Thomas L. Frölicher^{3,4}, Noel Keenlyside^{5,6}, Alistair J. Hobday⁷, Friedrich A. Burger^{3,4}, Piero S. Bernardo¹ & Julia Araújo¹

The impacts of marine heatwaves (MHWs) on marine ecosystems can be amplified when combined with other extreme events. Here, we investigate the spatiotemporal evolution of compound events of MHW, high acidity and low chlorophyll in the equatorial and South Atlantic, using observation-based datasets and reanalysis products. We show that the frequency and intensity of these triple compound events under a fixed baseline have increased dramatically over the past two decades, peaking in the most recent years. We analyse the drivers of triple compound events for six regions and find that, for the Angola Front and Brazil-Malvinas Confluence regions, these events are associated with a poleward shift of the fronts. In the Agulhas Leakage region, an increase in warmer waters entering from the Indian Ocean leads to compound extremes. In the western equatorial and subtropical Atlantic, they are caused by changes in the air-sea heat fluxes, while in the eastern equatorial by a weakening of upwelling. In addition, triple compound events are widespread over the South Atlantic during El Niño events, which is important because MHWs can be predicted when associated with ENSO.

Marine heatwaves (MHWs)^{1,2} can have devastating effects on marine ecosystems, ranging from habitat shifts³ and changes in population structure to high mortality of various marine species^{4–6}. These extreme events may thus overwhelm the capacity of both natural and human systems to cope, causing socioeconomic impacts, such as loss of essential ecosystem services and fisheries income^{7,8}. The frequency and severity of MHWs relative to a historical baseline have increased over the last century mainly due to anthropogenic climate change^{9–11} and will continue to do so as global temperatures continue to rise unabated^{9,12–14} with potentially widespread consequences for marine ecosystems globally.

The impacts of MHWs can be amplified when combined with other extreme events, such as low productivity and high acidity (OAX) events that can act synergistically¹⁵. As the ocean warms during an MHW in low- and mid-latitude regions, the shoaling of the

mixed-layer depth inhibits the flow of nutrient-rich waters into the euphotic zone, decreasing primary productivity^{16–18}. In addition, the oceanic uptake of anthropogenic CO₂ leads to an increase in hydrogen ion concentration [H⁺], a reduction in the pH of seawater (acidification) and an associated increase in ocean acidity extreme events¹⁹, with potentially devastating consequences for marine ecosystems²⁰. An increase in temperature during an MHW can cause a direct rise in [H⁺] via changes in the carbonate chemistry equilibrium²¹ and an indirect decrease in [H⁺] by reducing the CO₂ solubility in surface waters or decreasing the upwelling of carbon-rich deep waters to the surface²². The former often overwhelms the latter mainly in the subtropics²³. Ocean warming during an MHW in these regions leads to an increase in [H⁺] and thus to acidification. Most of our knowledge comes from the impacts of individual univariate extreme events²⁴. However, recent studies discussed the

¹Department of Oceanography, Federal University of Santa Catarina, Florianópolis, SC, Brazil. ²Laboratoire LOCEAN-IPSL, Sorbonne Université, Paris, France.

³Climate and Environmental Physics, Physics Institute, University of Bern, Bern, Switzerland. ⁴Oeschger Centre for Climate Change Research, University of Bern, Bern, Switzerland. ⁵Geophysical Institute, Bjerknes Centre for Climate Research, University of Bergen, Bergen, Norway. ⁶Nansen Environmental and Remote Sensing Center, Bergen, Norway. ⁷CSIRO Environment, Hobart, TAS, Australia. ✉e-mail: regina.rodrigues@ufsc.br

potentially devastating effect of multivariate compound extremes on marine ecosystems^{17,25,26}.

To guide adaptation and mitigation policies to avert the most severe impacts on marine ecosystems, it is essential to improve the understanding of the physical drivers of these marine compound extreme events and our ability to predict them²⁷. However, many studies in the last decade have focused only on the drivers of MHWs or other extremes independently. MHWs can be forced by atmospheric and oceanic processes depending on the location and seasonality^{28–31}. For instance, a large proportion of the most extreme extra-tropical MHW events are driven by persistent high-pressure systems and weaker winds that lead to increased insolation and reduced ocean heat losses³². This mechanism was responsible for several unprecedented events, including those in the Mediterranean Sea during the summer of 2003³³, in the northwest Atlantic in 2012³⁴ and in the southwest Atlantic during the austral summer of 2013/14³⁵. MHWs can also be generated by increased ocean transport of heat, such as the 2011 eastern Australia MHW¹ and reduced coastal upwelling in the event of the Peruvian coast in 2017³⁶. A combination of multiple interacting mechanisms can also lead to extreme MHWs, such as the notorious North Pacific Blob³⁷.

Despite the size and importance of the region, few studies have focused on MHWs in the equatorial and South Atlantic^{13,35,38}. These studies find that MHWs in the southwestern South Atlantic are driven mainly by persistent high-pressure systems that inhibit convection, decreasing cloud cover and increasing the input of shortwave radiation to the ocean. Often, the atmospheric anomalies are remotely caused via teleconnections from the Indian and Pacific oceans linked to modes of climate variability. Moreover, MHWs have intensified in the last four decades, and their frequency, intensity and duration are projected to increase in the future¹³. There is some evidence that MHWs have already had a negative impact on marine life in the southwestern South Atlantic³⁹. However, there are no studies on MHWs or compound events for the most biologically productive areas

in the equatorial and South Atlantic, such as the Benguela/Agulhas region, Brazil–Malvinas confluence, Angola Front and equatorial Atlantic. Combined, these regions are responsible for annual catches of about 8 million tonnes of marine organisms that support many South American and African coastal communities⁴⁰.

Here, we investigate the spatiotemporal evolution of compound events of MHW, OAX, and low chlorophyll (LChlX) in the equatorial and South Atlantic, using observational-based datasets and reanalysis products. The common drivers of triple compound events are investigated in biologically productive open ocean areas of the equatorial and South Atlantic that present strong positive trends in MHW cumulative intensity and an increase in the occurrence of compound extremes.

Results

MHWs in the South Atlantic

To address the knowledge gap for MHWs in the equatorial and South Atlantic, we first analysed the spatial patterns and temporal evolution of the MHWs from 1982 to 2020, comparing them with changes in sea surface temperature (SST). We define MHWs and all other extremes here relative to a fixed seasonally varying climatological baseline (see Methods). The long-term linear trends in both SST and MHW cumulative intensity are positive in almost the entire South Atlantic during austral summer (DJF, Fig. 1) when the SST is already at its seasonal maximum and thus near the thermal limit of many species in the region⁴¹. Weaker but similar trends are observed in annual averages of SST and MHW cumulative intensity (Fig. S1). Negative trends appear only on the northern edge of the subtropical gyre and a few spots on the southern edge of the domain, but they are not statistically significant.

The areas where the SST rises at the fastest rates are not necessarily where the extreme temperatures (MHWs) intensify, despite apparently similar spatial patterns. The strongest positive trends in SST exceeding 0.4 °C per decade are observed on the eastern side of

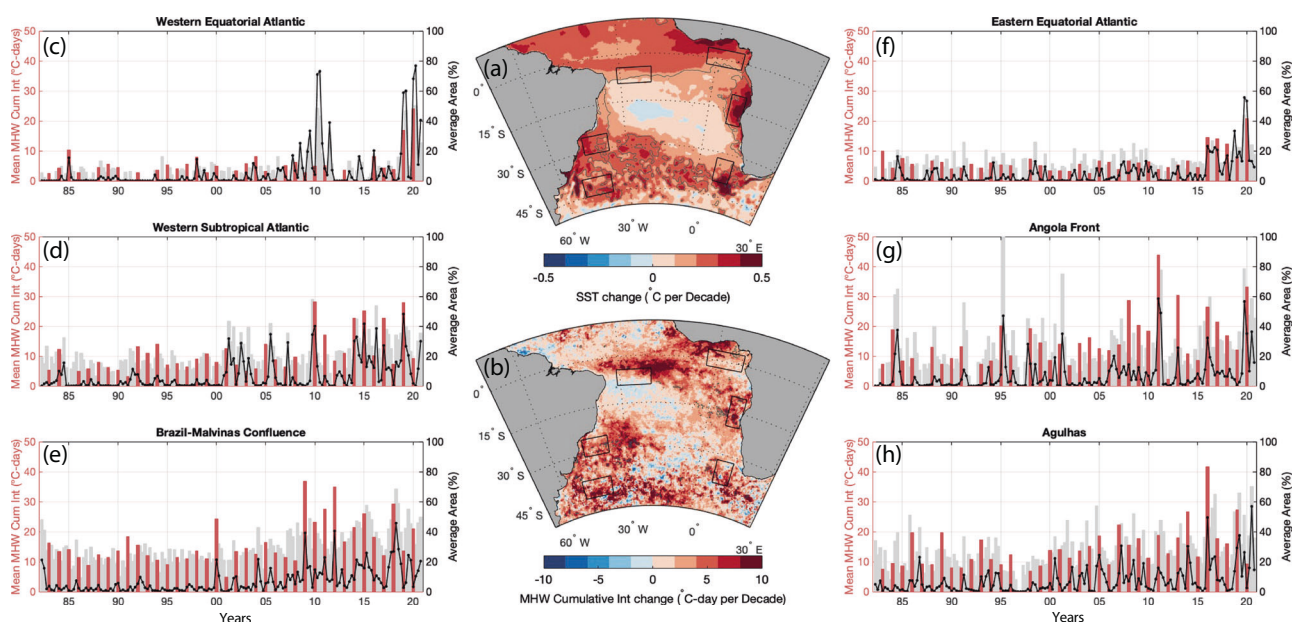


Fig. 1 | Long-term changes in sea surface temperature and marine heatwaves in the South Atlantic. Maps of linear trends in austral summer (December–February, DJF) for 1982–2020: **a** sea surface temperature (SST) and **b** marine heatwave cumulative intensity. **c–h** Time series of monthly marine heatwave cumulative intensity (bars, left y-axis) and marine heatwave spatial coverage (black solid lines, right y-axis) for the six regions highlighted by black boxes on the maps: **c** western

equatorial Atlantic, **d** western subtropical South Atlantic, **e** Brazil–Malvinas confluence, **f** eastern equatorial Atlantic, **g** Angola Front and **h** Agulhas Leakage. Grey bars display monthly averages for all months, and red bars for summer months only (DJF). Solid lines in **a** and **b** encompass areas where the trends are statistically significant at the 95% confidence level given by the non-parametric Mann–Kendall test.

the basin, such as in the Gulf of Guinea, Angola Front and Agulhas Leakage (Fig. 1a). In contrast, the strongest positive trends in MHW cumulative intensity, surpassing 10 °C-day per decade, tend to occur on the western side of the basin, such as in the western equatorial Atlantic, western subtropical Atlantic and the Brazil-Malvinas Confluence region (Fig. 1b). Nevertheless, MHW trends are also high in the Gulf of Guinea, Angola Front and Agulhas Leakage.

Analysing the monthly time series of MHW cumulative intensity and coverage area for the six selected regions with high MHW trends shows that MHWs have become more intense, frequent and larger, particularly in the last two decades (Fig. 1c–h; note that the time series covers all seasons with the red bars representing summer). For instance, the western equatorial Atlantic had not experienced months with more than 10 °C-day and 10% of MHW coverage before 2000 (Fig. 1c). Over the last two decades, stronger and larger events became more common with two notable MHWs happening around 2010 and 2020. During these two events, cumulative intensity and coverage area reached nearly 25 °C-day and 75%, respectively. A similar pattern occurs in both the western subtropical South Atlantic (Fig. 1d) and the Brazil–Malvinas confluence (Fig. 1e), where the intensity and area of the MHWs did not exceed, respectively, 20 °C-day and 20% before 2000. This is particularly evident during austral summer (red bars in Fig. 1c–e). Moreover, along the western South Atlantic, MHWs have become not only more frequent but also more persistent (Fig. S1c,d). For the western equatorial Atlantic, the MHW events are up to 6 days longer per decade (Fig. S1d), with an increase in frequency between 10 and 30 days per year per decade (Fig. S1c).

On the eastern side of the basin, MHW events also became stronger and more extensive after 2000, particularly in austral summer for Angola Front and Agulhas regions (red bars in Fig. 1g,h). In the eastern equatorial Atlantic near the Gulf of Guinea (Fig. 1f), cumulative intensity and coverage area did not exceed 10 °C-day and 10%, respectively, before 2015. The largest MHW reached over 20 °C-day and covered more than half of the area in 2020. In the Angola Front, the largest and most intense summer MHW occurred in 2011 (Fig. 1g). The strongest events before 2000, such as the events of 1984 and 1995, occurred during other seasons. Similarly, for the Agulhas Leakage region (Fig. 1h), MHWs have become stronger and larger in recent years during austral summer, with the strongest event occurring in 2016. Along the eastern South Atlantic, MHWs have become more frequent everywhere by up to 15 days per year per decade (Fig. S1c). However, the pattern in duration is different from the western South Atlantic, apart from the Agulhas Leakage (Fig. S1d). There has been a decline in their duration in the Angola Front and a slight increase in the eastern equatorial Atlantic (Fig. 1d).

Compound events in the South Atlantic

Next, we described the compound events of coincident MHW, OAX, and LChIX expression for the period from 1999 to 2018 (see Data and Methods for more details). There has been a widespread increase in the occurrence of triple compound events in the South Atlantic (positive values in Fig. 2a), including the six selected areas. (See more details on how these regions are defined in the Methods). Triple compound events were rare from 1999 to 2008 but became increasingly common from 2009 to 2018 (Fig. S2a,d). This is mainly because OAX events are practically non-existent in the former period (Fig. 2f and S3c,f). Nonetheless, MHWs have also become more frequent in the last decade in the equatorial Atlantic and on the western side and southern edge of the subtropical gyre (Fig. 2d and S3a,d). Combined with MHW, LChIX became more frequent in the equatorial South Atlantic (Fig. 2b and S2b,e), where the increase in LChIX (Fig. 2e) partially overlaps with that in MHWs (Fig. 2d). Double compound events of MHW and OAX have increased over the whole of the South Atlantic (Fig. 2c and S2c,f) mainly due to the widespread increase in OAX (Fig. 2f and S3c,f).

We also analysed the temporal evolution of the triple compound events in the selected areas for 1999–2018 (Fig. 3). For reference, the time series of the individual events of MHW, OAX and LChIX are displayed for the six selected regions in Figs. S4–S9. Note that we consider a triple compound event when the extremes occur simultaneously and overlap in at least 1% of the area within the boxes in Fig. 1 (asterisks in Fig. 3). In all selected regions, there were no triple compound events during the first decade that overlapped at least 1% of the area in question (1999–2008). For most regions, this is because events of OAX were rare in the first decade, except for the Angola Front. In the western equatorial Atlantic, the occurrence of triple compound events went from 0 during 1999–2008 to 17 months per decade during 2009–2018 (Fig. 3a and S4), with combined intensity surpassing 4 standard deviations in some months. In the western subtropical South Atlantic, there was an increase from 0 to 37 months in their occurrence (Fig. 3b and S5). In 2014 and 2016, the area of overlap reached more than 30% of the region, with combined intensity surpassing 3 standard deviations. A similar pattern was found for the Brazil-confluence region, with an increase from 0 to 39 months per decade, with 2018 presenting almost 60% of the area covered by the triple compound with a combined intensity of almost 4 standard deviations (Fig. 3c and S6). On the eastern side of the basin, the occurrence of triple compound events went from 0 to 40 months per decade in the equatorial Atlantic (Fig. 3d and S7), from 3 to 49 months per decade in the Angola Front (Fig. 3e and S8), and from 0 to 22 months per decade in the Agulhas Leakage region (Fig. 3f and S9). The summer of 2015/2016 was exceptional in terms of spatial coverage and intensity of triple compounds for all regions. (See also Tables S1–S6 for the detailed changes in all regions, including individual and double compound extremes.)

Events of OAX and LChIX are not independent of MHWs^{17,23}, as MHWs tend to lead to a decrease in chlorophyll in the low to mid-latitudes and, up to a certain point, to an increase in acidification. While the increase in acidity is a direct thermodynamic effect of the warming, the decrease in chlorophyll can be a result of a decrease in nutrients and due to the physical mechanisms (drivers), as shown in the next section. We quantify the dependence between two extreme events when they occur together using the likelihood multiplication factor (LMF)^{17,23}, which measures how many times more/less frequent compound events are compared to their expected frequency under the assumption of independence (see Methods for more details). We start with the double compound events of MHW and OAX (Fig. 2g, Tab. S7). Regions where LFM is different from one indicate that MHWs and OAX events co-occur more often ($LMF > 1$, red shades in Fig. 2g) or less often ($LMF < 1$, blue shades in Fig. 2g) than if variations in SST and $[H^+]$ anomalies were independent ($LMF = 1$). Their interdependence is positive mainly in the equatorial Atlantic and subtropical South Atlantic and negative in higher latitudes of the South Atlantic (Fig. 2g, Tab. S7). Double compound events of MHW and LChIX (Fig. 2h, Tab. S8) are positively interdependent mainly in the subtropical South Atlantic, along the edges in the middle and eastern side of the basin. In contrast, double compound events of OAX and LChIX are positively interdependent in the western boundary (Fig. 2i, Tab. S9). Within our six selected regions, double compounds are mostly positively dependent on each other (Tabs 7–9). One needs to investigate their drives to understand the reason for their interrelationship. This will be addressed in the next section.

Here, extreme events are defined relative to a fixed baseline, given the short period analysed (two decades). However, since acidity levels strongly increased over this period (Figs. S4–S9), we have repeated the analysis detrending all three datasets with a linear fit (Figs. S10–S12). Comparing Fig. 2 and S10, the changes in extremes are spatially consistent. There are very few differences in the triple and double compound extreme events everywhere, particularly within the selected regions (Fig. S10a–c). The areas with a stronger increase in the

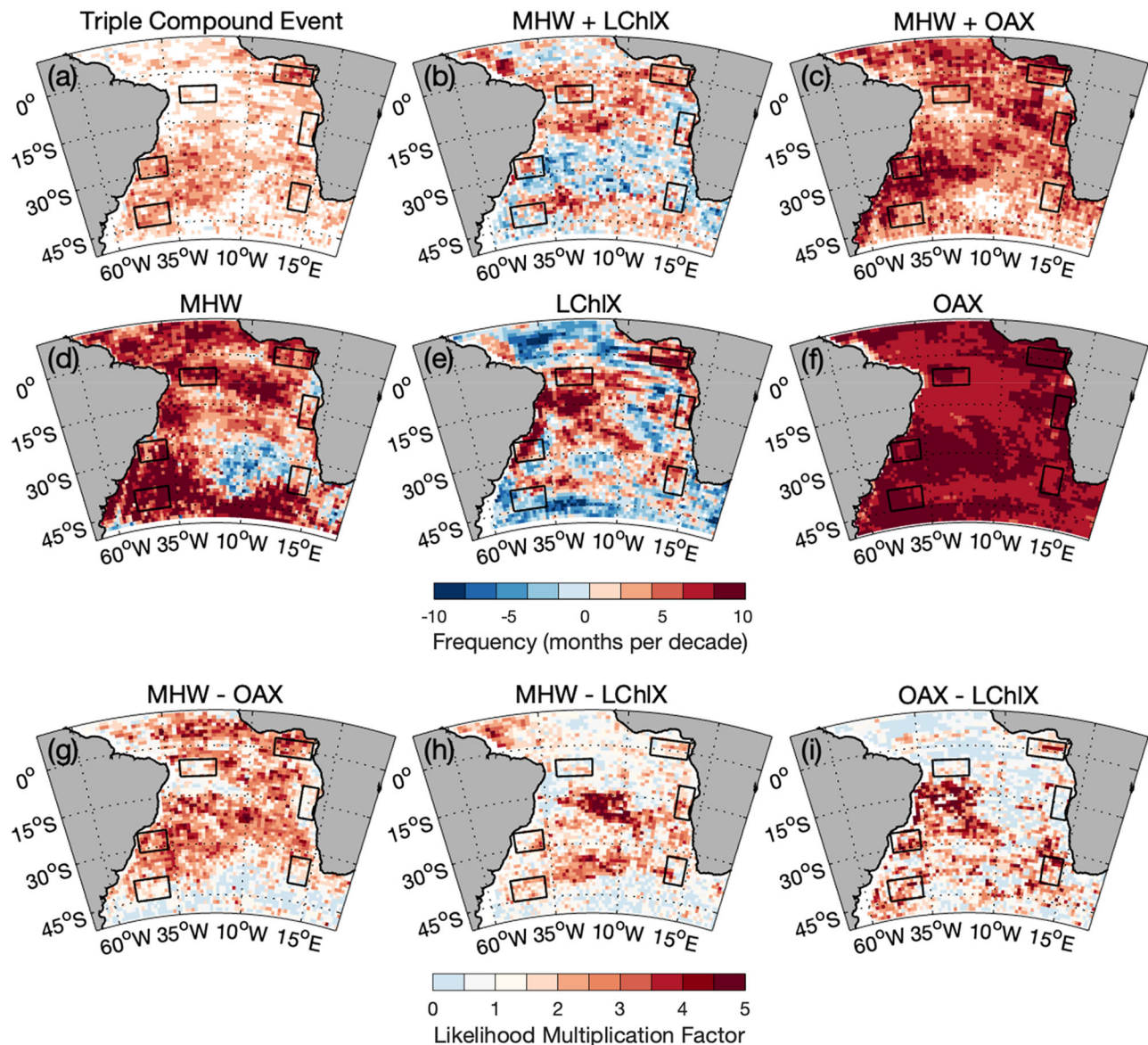


Fig. 2 | Changes in marine heatwaves and compound events in the South Atlantic. Change in the frequency of **a** triple compound events (MHW+LChIX +OAX), **b** marine heatwave (MHW) + low chlorophyll (LChIX), **c** marine heatwave (MHW) + high acidity (OAX), **d** marine heatwave (MHW), **e** low chlorophyll (LChIX) and **f** high acidity (OAX) in the equatorial and South Atlantic, represented as the

difference between 1999–2008 and 2009–2018. Likelihood multiplication factor for double compound events of **g** MHW and OAX, **h** MHW and LChIX and **i** OAX and LChIX, considering the entire period (1999–2018). As in Fig. 1, the black boxes highlight the six regions.

occurrence of extreme events continue to present, in general, a positive increase, albeit weaker. Double compound events of MHWs and LChIX are remarkably similar (Fig. S10b). In fact, LChIX events obtained from the detrended data appear to be more frequent in the second decade in some regions (Fig. S10e), such as along the southern edge of the subtropical gyre, including the Brazil–Malvinas confluence. This is consistent with increased chlorophyll levels in higher latitudes due to ocean warming, described in the literature³². There are regions now where triple and double compound events of MHWs and OAX slightly decrease (blue shading in Fig. S10c) after removing the pronounced [H⁺] trend, reflecting a reduction in OAX events (Fig. S10f). However, the results for MHWs detrending the data present few differences in the South Atlantic compared to those with the trend (Figs. S10d and 2d, respectively), except for the tropical North Atlantic. This reflects the different patterns in the long-term trends between SST and MHW cumulative intensity (Fig. 1a,b). Therefore, this comparison gives us confidence in detecting extremes relative to a fixed baseline.

Local drivers of triple compound events

Now, we investigate the local physical mechanisms that lead to triple compound events in the selected areas of the equatorial and South Atlantic: air–sea interaction is responsible for triple compound events in the western equatorial Atlantic and western subtropical Atlantic, weakening of upwelling in the eastern equatorial Atlantic, latitudinal shifts of fronts in the Angola Front and Brazil–Malvinas confluence regions and eddy trapping in the Agulhas Leakage region. These local mechanisms have been reported in the literature as drivers of MHWs^{28,32} and also the potential drivers of triple compound events of MHWs, OAX and low oxygen for the Northeast Pacific²⁵ (see Fig. 3).

To reveal the main drivers of triple compound events in the selected areas, we construct composites of atmosphere and ocean fields from reanalysis products and present the differences between summer months (DJF) with triple compound events and those without, except for the western equatorial Atlantic where we use autumn months (see Methods for more details). Note that MHWs occur during

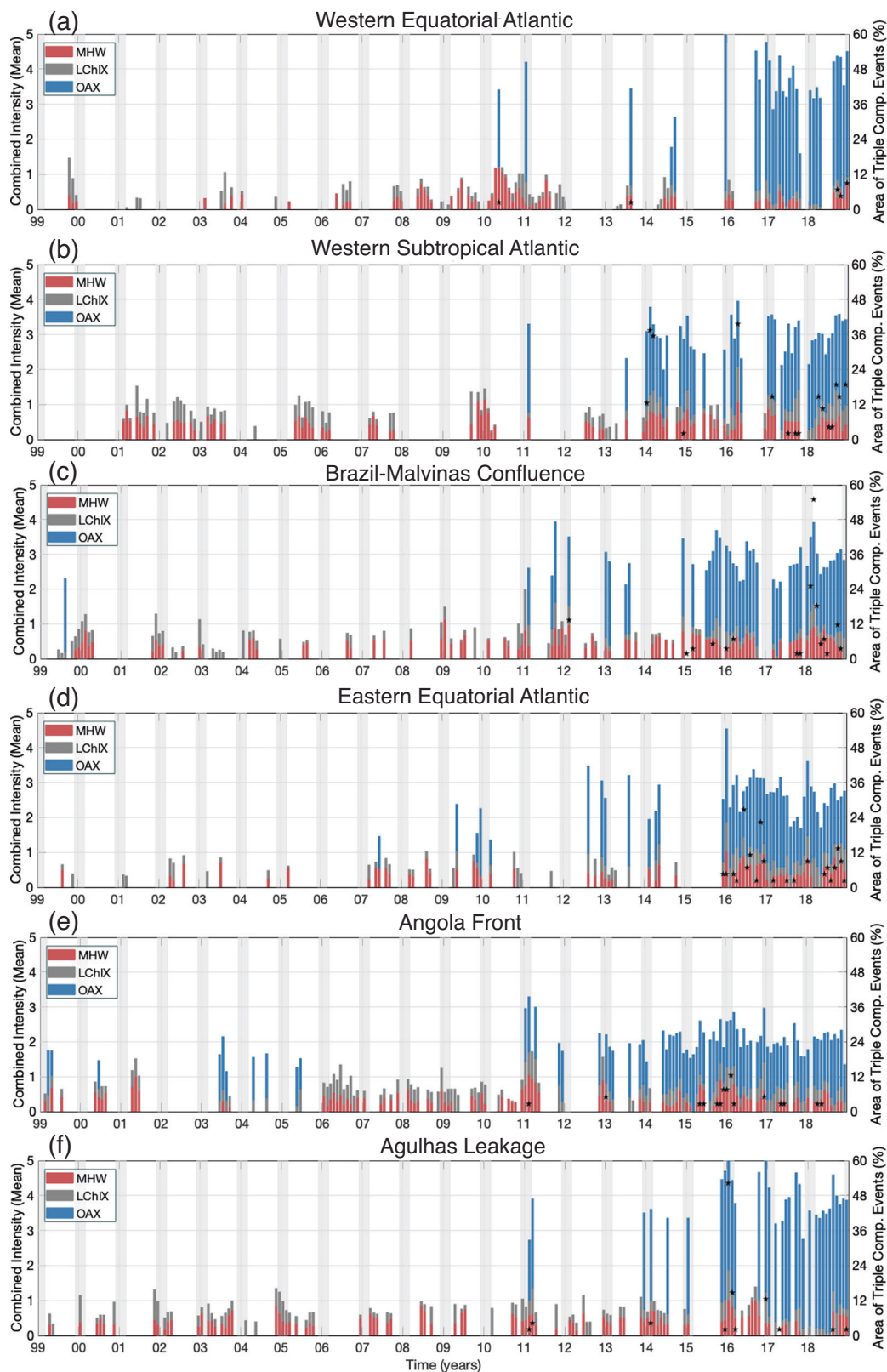


Fig. 3 | Mean triple compound event intensity and area coverage by region. The normalised monthly intensity of marine heatwaves (MHW, red), extreme events of low chlorophyll (LChIX, grey) and high acidity (OAX, blue) averaged over: **a** western equatorial Atlantic, **b** western subtropical South Atlantic, **c** Brazil–Malvinas confluence, **d** eastern equatorial Atlantic, **e** Angola Front and

f Agulhas Leakage. Marine heatwaves and events of low chlorophyll are calculated from daily data, and the monthly values represent the cumulative intensity over each month. Values displayed are normalised by their standard deviation. Asterisks indicate the area covered by triple compound events in each region (in percentage, right y-axis).

summer (or autumn) months without triple compound events for all selected areas (see Fig. 3). Thus, the mechanisms described here are related to triple compound events and not just MHWs. Our understanding is that the mechanisms leading to the MHWs described in this section are also conducive to OAX and LChIX events based on the LMF results in the previous section.

The weakening of the southeasterly trades in the western equatorial Atlantic (vectors in Fig. 4c) causes a decrease in evaporative cooling or latent heat loss from the ocean to the atmosphere (positive anomalies represented by red shading in Fig. 4c), warming the ocean. For reference, the climatological wind field over the equatorial and South Atlantic is shown in Fig. S13a. This thermodynamic feedback, known as the wind-evaporation-SST (WES) mechanism, has been described as the main process driving changes in SST in the tropical Atlantic⁴² (Fig. 4a). The warming together with the weakening of the winds leads to the shallowing of the mixed layer (negative anomalies represented by blue shading in Fig. S14a), enhancing upper-ocean stratification. This, in turn, inhibits mixing with deeper layers and reduces nutrient inputs to the mixed layer. Consequently, surface chlorophyll concentration declines and events of LChIX increase (LMF > 1 in Fig. 2h, Table S8). Moreover, the horizontal advection of upwelled rich-in-nutrient waters from the eastern to the western side of the basin is reduced over the area (westward currents, vectors in Fig. S14a) due to the weakening of the trade winds. Note that this region within the Atlantic warm pool is already considered oligotrophic, i.e., poor in nutrients. The decline in chlorophyll concentration could lead, in turn, to a reduction of organic matter production and, therefore, to more inorganic carbon and higher acidity in surface waters. However, stronger positive interdependence is found between MHW and OAX than between OAX and LChIX (LMF > 1 in Fig. 2g, i, Tables S7 and S8, respectively).

In the western subtropical South Atlantic, the presence of a persistent high-pressure system represented by an anticlockwise circulation (vectors in Fig. 4d) is associated with triple compound events. In this case, ocean warming is caused mainly by an increase in shortwave radiation at the ocean's surface (positive anomalies represented by red shading in Fig. 4d). The high-pressure system suppresses convection and decreases cloud cover over the region (negative anomalies represented by dashed contours in Fig. 4d), with changes in latent heat flux playing a minor role. This mechanism has been reported as the primary driver of MHWs in this region³⁵ (Fig. 4a). Similar to the western equatorial Atlantic, the warming also leads to the shoaling of the mixed-layer depth, enhancing stratification that further intensifies the warming. Consequently, MHWs that develop in this region increase acidity levels, and strong stratification prevents the mixing of nutrient-rich waters, leading to triple compound events. This is corroborated by the LMF analysis that shows strong positive interdependence among the three extremes (LMF > 1 in Fig. 2g–i, Tabs. S7–S9). Notably, compound MHW and OAX events occur more often in the western subtropical region compared to the western equatorial region (cf. Tables S1 and S2), in line with previous results showing generally high frequency of MHW and OAX events in subtropical oceans where $[H^+]$ is particularly temperature driven²³.

Along the eastern equatorial Atlantic, a reduction of the equatorial upwelling is responsible for the triple compound events. The weakening of the trade winds in the equatorial Atlantic can decrease the upwelling of cold waters along the eastern equatorial Atlantic via Bjerknes feedback⁴³, causing warming (Fig. 4b). This process is similar to what happens in the equatorial Pacific during El Niño events and has been described as the driver of the Atlantic Niño⁴⁴. While the Bjerknes feedback is more active in austral winter, it can occur during summer, the period when our analyses are made⁴⁵. Indeed, triple compound events in the eastern equatorial Atlantic are associated with a weakening of the southerly trades (vectors in Fig. 4e), leading to a deepening of the thermocline in the eastern equatorial Atlantic (positive

anomalies represented by red shading in Fig. 4e) and a shallowing of the thermocline in the western equatorial Atlantic (negative anomalies represented by blue shading in Fig. 4e). Note that this is the opposite for the mixed-layer depth (shading in Fig. S14b). This means that less cold and rich in nutrients and carbon, subsurface waters reach the surface, leading to LChIX levels and, in principle, low acidity levels. However, the warming effect on $[H^+]$ overcompensates the carbon effects and leads to higher H^+ concentrations, even though the upwelling of carbon-rich subsurface waters is weaker²³. The advection of warm, acid and poor-in-nutrient waters from the western side of the basin to the area also helps to produce the triple compound events (vectors in Fig. S14b). Consequently, the waters are warmer and have OAX and LChIX levels. These changes are interdependent (LMF > 1 in Fig. 2g–i, Tables S7–S9).

The Brazil–Malvinas confluence is characterised by a sharp meridional temperature gradient located around 37°S and separates the warmer waters brought by the Brazil current from the cold waters transported northward by the Malvinas current (Fig. 5a). The poleward intrusion of warm tropical waters carried by the Brazil current shifts the front, causing warming of the region. Moreover, the Brazil current carries nutrient-poor and high-acidity waters when compared to the waters from the Malvinas current (respectively Fig. S15a, c). Here, we show that widespread and intense triple compound events in the region during summer (Fig. 3c) are associated with strong poleward shifts in the Brazil–Malvinas confluence (Fig. 5c), mainly in 2012, 2016, and 2018. The position of the confluence is computed as the location of the maximum SST gradient along the 1000-m isobath between 34°S and 41°S⁴⁶. This is consistent with a poleward migration of the South Atlantic subtropical high (Fig. S13b) that favours the advection of warm, carbon-rich, and nutrient-poor waters from the Brazil current while inhibiting the advection of cold, carbon-poor and nutrient-rich waters from the Malvinas current, leading to the triple compound events in the region. Again, their interdependence is corroborated by the LMF analysis (LMF > 1 in Fig. 2g–i, Tables S7–S9).

Similarly, the Angola Front is a sharp meridional temperature gradient located around 15°S and separates the warm tropical waters in the north from the cold upwelled waters in the south (Fig. 5b). Warming in this region is generally associated with the poleward intrusion of warm tropical waters transported by the Angola current, associated with coastally trapped waves (Fig. S14c), and a reduction in the coastal upwelling in the south, caused mainly by a weakening of the alongshore winds from the south^{47–49}. This mechanism can be depicted as a southward shift of the front position, so here we computed the latitudinal position of the Angola Front (Fig. 5d) as the location of the maximum SST gradient along the 10° E meridian⁵⁰. The southward shift of warm, nutrient-poor, and high-acidity waters forms the triple compound events in the Angola Front region (respectively Fig. 5b and Fig. S15b,d). Widespread and intense triple compound events in the region during summer (Fig. 3e) tend to be preceded by strong southward shifts in the Angola Front (Fig. 5d). The most extreme summers of 2010/11 and 2015/16 in terms of triple compound events present the most extreme southmost excursions of the Angola Front on record. In this region, a stronger positive interdependence is only found between MHW and LChIX (LMF > 1 in Fig. 2h, Tab. S8), with weak but still mostly positive interdependence between MHW and OAX (LMF > 1 in Fig. 2g, Tab. S7), probably due to the advection effect rather than reduction in the upwelling. In contrast with the eastern equatorial Atlantic, here the warming effect on $[H^+]$ does not overcompensate the carbon effects. Thus, the weakening of the upwelling leads to less carbon-rich and nutrient-poor subsurface waters being upwelled. Consequently, OAX and LChIX events are negatively interdependent (LMF < 1 in Fig. 2i, Tab. S9).

The Agulhas leakage region is characterised by the inflow of warm and saline waters from the Indian Ocean into the South Atlantic via the shedding of anticyclonic Agulhas rings and direct inflow, both

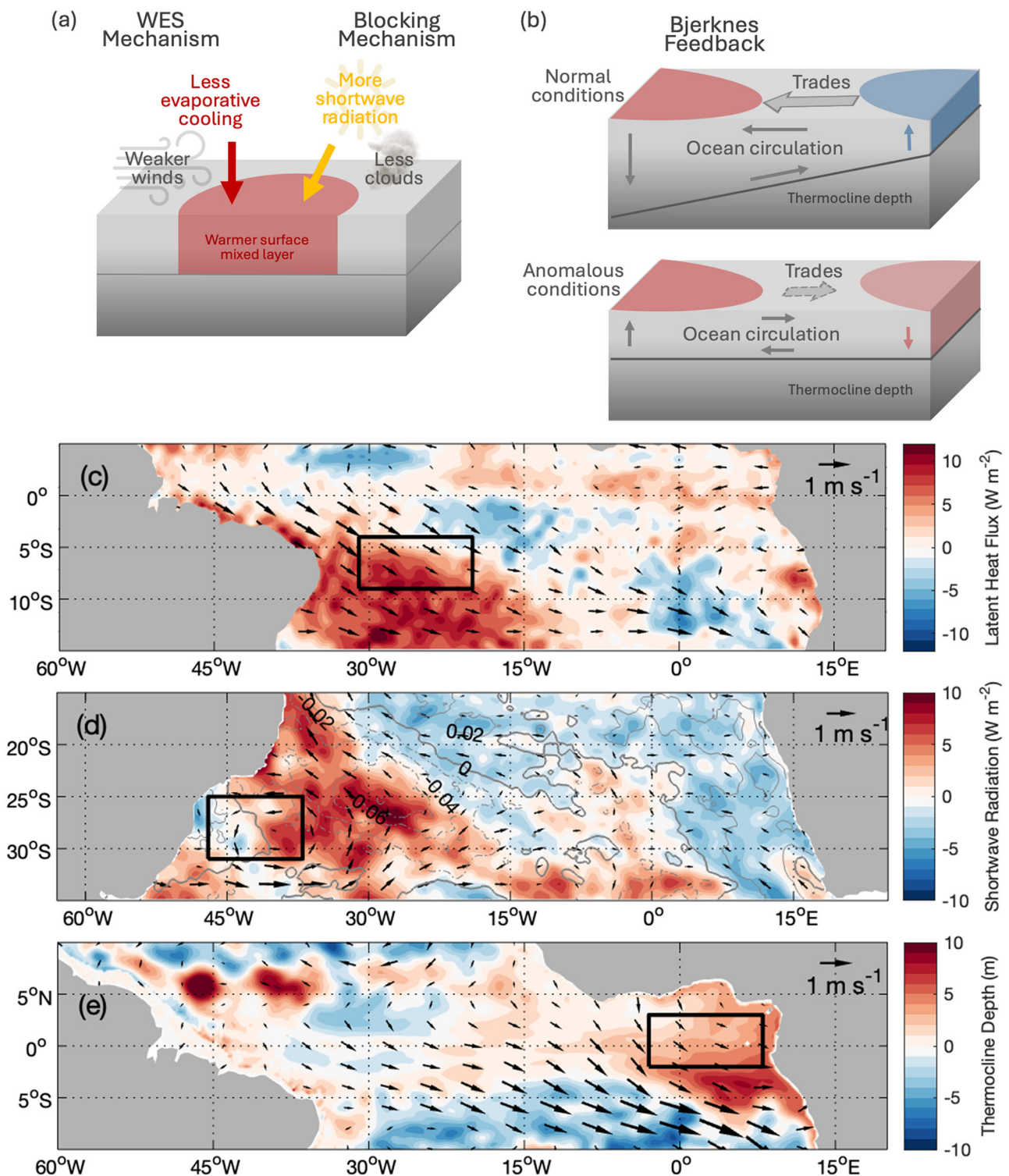


Fig. 4 | Air-sea interaction and ocean dynamics as the primary driver of triple compound events. **a** Schematic of the wind-evaporation-SST (WES, left) and atmospheric blocking (right) mechanisms. **b** Schematic of the Bjerknes feedback. **c** Composite of the anomalies of wind (vectors, m s^{-1}) and latent heat flux (shading, W m^{-2}) for the triple compound events in the western equatorial Atlantic region (black box). **d** Composite of the anomalies of wind (vectors, m s^{-1}), shortwave radiation (shading, W m^{-2}) and cloud cover (contours, %) for the triple compound

events in the western subtropical Atlantic region (black box). **e** Composite of the anomalies of wind (vectors, m s^{-1}) and thermocline depth (shading, m) for the triple compound events in the eastern equatorial Atlantic region (black box). Solid and dashed lines in **(d)** depict positive and negative anomalies, respectively, with the tick solid line representing the 0 contour and contour interval every 2% of cloud cover. See methods for more details on how the composites are calculated.

associated with the retroflexion of the Agulhas current (Fig. 6a). Triple compound events in the Agulhas Leakage region are also associated with a southward shift of the South Atlantic subtropical high, strengthening easterly winds along the southern tip of Africa (vectors

in Fig. 6c). This enhances the leakage of warmer waters from the Indian Ocean into the eastern South Atlantic. In addition, the associated weakening of upwelling-favourable winds along Southern Benguela deepens the thermocline (positive anomalies represented by red

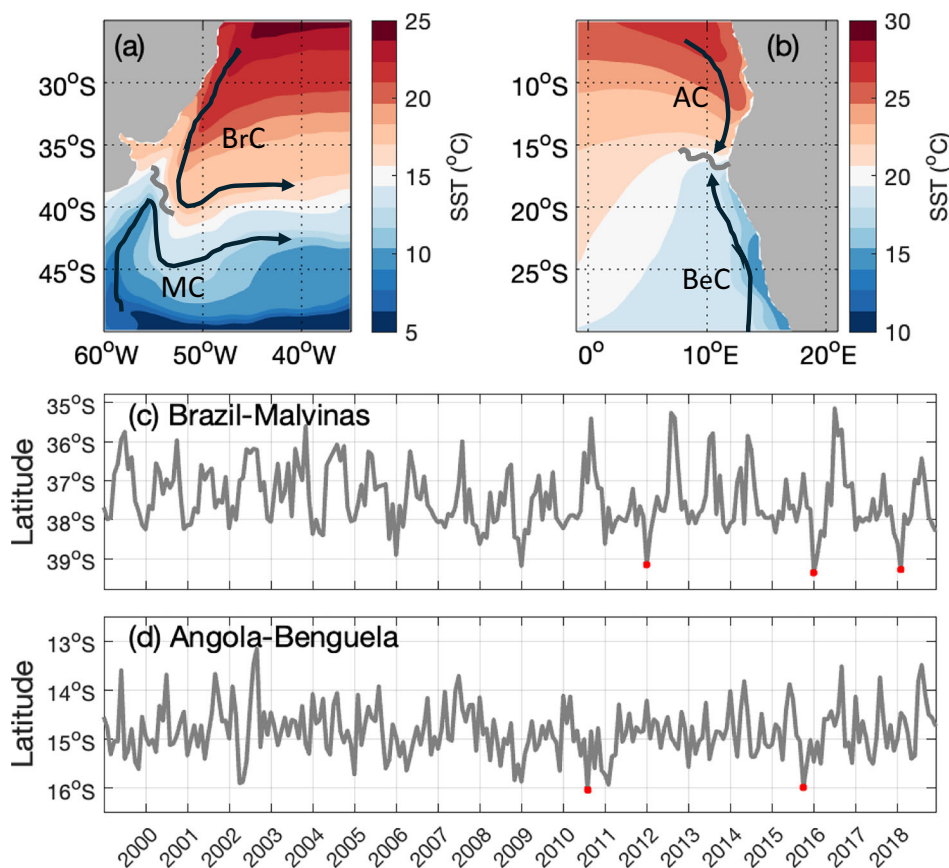


Fig. 5 | Latitudinal shifts of fronts as the primary driver of triple compound events. Schematic of the Brazil–Malvinas confluence front characterised by a sharp SST gradient (shading) separating the warmer waters of the Brazil current (BrC) from the cold waters of the Malvinas current (MC). **b** Same as **a**, except for the Angola–Benguela Front separating the warmer waters of the Angola current (AC)

from the cold waters of the Benguela current (BeC). Latitudinal position of **c** Brazil–Malvinas confluence and **d** Angola Front, computed as the location of the maximum SST gradient in degrees of latitude (see Methods). Red dots represent the years with widespread and intense triple compound events and record poleward shifts of the fronts.

shading in Fig. 6c), enhancing the warming over that region. Together, these processes contribute to the development of the MHW and the apport of nutrient-poor waters into the Agulhas leakage region. Moreover, anticyclonic Agulhas eddies forming in the region trap warm nutrient-poor waters, while cyclonic Agulhas eddies originate from the Benguela upwelling region and trap cold nutrient-rich waters^{51,52} (Fig. 6b). Warm anticyclonic eddies have higher $[H^+]$ concentrations when compared to surrounding waters because they absorb more CO_2 than the surrounding waters in the summer^{51–53}. The mesoscale modulation of CO_2 flux is driven by the balance between temperature and dissolved inorganic carbon (DIC) effects. Generally, warmer SST in anticyclonic eddies reduces the solubility, hence the pCO_2 increases. On the other hand, anomalously low DIC in anticyclones reduces pCO_2 , leading to more uptake during summer. This is because the DIC-driven effect is greater than the temperature-driven effect during summer⁵⁴. This is corroborated by values of LMF > 1 between MHW and OAX events (Fig. 2g, Tab. S7). Moreover, the time series of the number of eddies (Fig. 6d), their azimuthal speed (Fig. 6e), and the area covered by the eddies (Fig. 6f) show that during the major triple compound events of 2014 and 2016 (Fig. 3f), there are more anticyclonic eddies (red lines, Fig. 6d) and to a certain point spending more time with lower speed (red lines, Fig. 6e) covering a greater area in the region (red lines, Fig. 6f). In addition, there are fewer cold cyclonic eddies (blue lines). Note that since we are dealing with a few extreme events in this short record and the interannual variability of SST in the area is driven by different mechanisms, we do not expect the time series of MHW or triple compound events to be statistically

correlated to those of the eddy characteristics and have used the LMF analysis to account for their interdependence.

Remote driver of triple compound events

The year 2016 was atypical. While recent years have been trending warmer, mainly due to anthropogenic climate change, the 2015/16 El Niño contributed to 2016 being the single warmest year on record since 1850⁵⁵, until 2023, when another strong El Niño event occurred. The amplitude of the 2015/16 El Niño was comparable to the two previous extreme El Niño events in 1982/83 and 1997/98⁵⁶, with widespread impacts affecting over 60 million people globally and requiring nearly US\$3.6 billion in humanitarian response⁵⁷. This event caused impacts regionally, such as the record marine heatwave off the coast of Alaska⁵⁸ and the record heat across Asia⁵⁹. While the impact of El Niño in terms of extremes over land is well documented, it is less so for ocean extremes, particularly in the equatorial and South Atlantic.

In 2015/16, the South Atlantic exhibited widespread extreme compound events. For example, 27% of all-time triple compound cumulative intensity and 28% of triple compound coverage area occurred in 2016 (Fig. S16). Triple compound events were also widespread during the weak El Niño of 2017/18. However, most of those events in 2018 occurred within the oligotrophic waters of the subtropical gyre and not within our selected regions, except for the Brazil–Malvinas Confluence (Fig. 3c). In contrast, most of the triple compound events in 2016 occurred in ecologically rich areas near the continental shelf of South America and Africa, including the six regions analysed here (Fig. S16). The percentage of the total area that

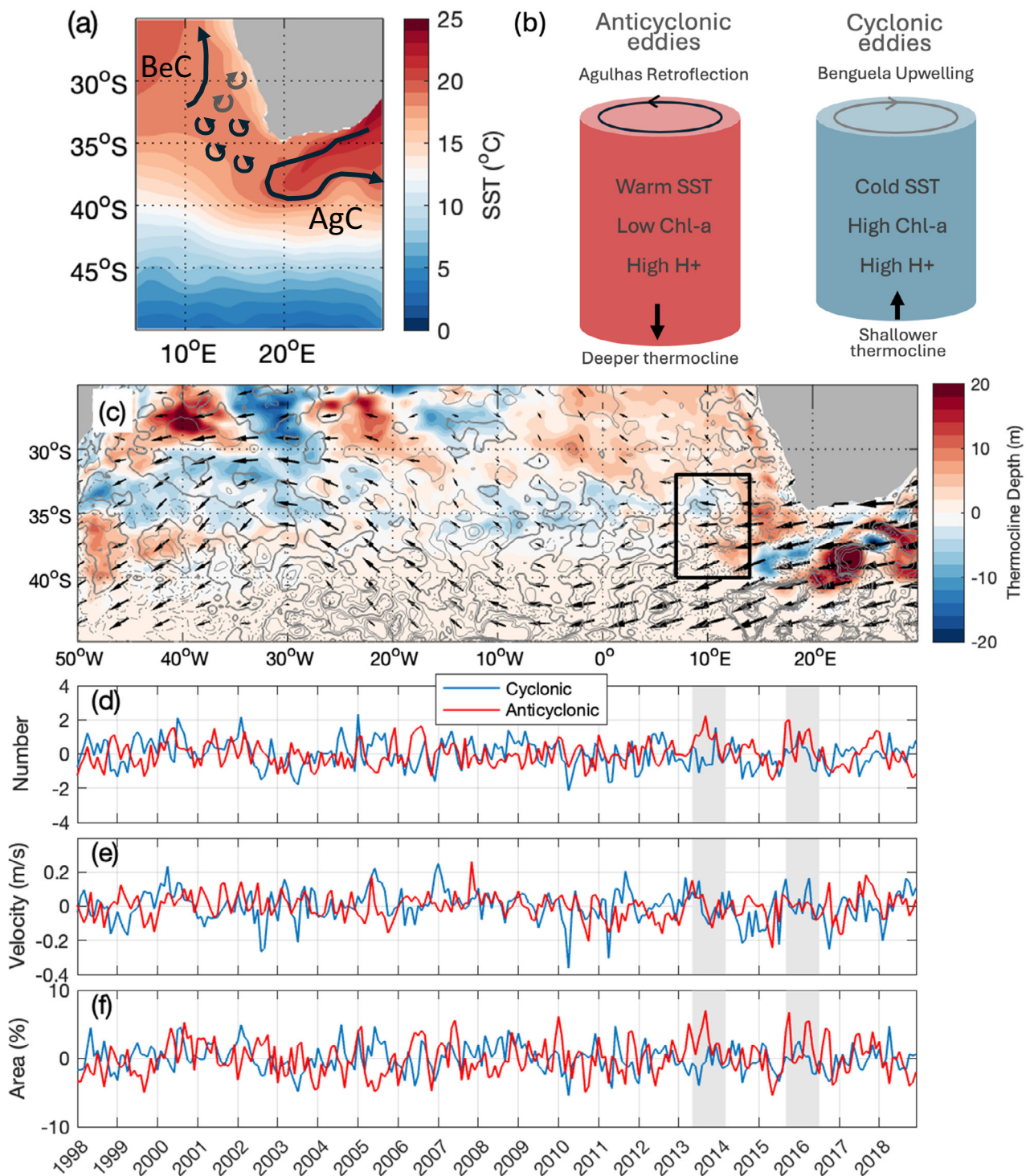


Fig. 6 | Eddy trapping as the primary driver of triple compound events.

a Schematic of the Agulhas current (AgC) retroflexion and leakage of warmer waters into the South Atlantic (shading, °C), anticyclonic (black) and cyclonic (grey) eddies and Benguela current (BeC). **b** Schematic of anticyclonic eddies trapping warm nutrient-poor waters from the Indian Ocean and cyclonic eddies trapping cold nutrient-rich waters from the Benguela Upwelling region. **c** Composite of anomalies of wind (vectors, m/s), thermocline depth (shading, m) and mixed-layer

depth (contours, m) for the triple compound events in the Agulhas Leakage region (black box). Time series of **d** the number of eddies, **e** azimuthal speed of eddies (m/s) and **f** the area covered by the eddies (%). Solid and dashed lines in (c) depict positive and negative anomalies, respectively, with the tick solid line representing the 0 contour and contour interval every 2 m of mixed-layer depth. Grey patches in (d-e) highlight the events of 2014 and 2016.

experienced simultaneously triple compound events in 2016 was 0% in the western equatorial Atlantic, 40% in the western subtropical South Atlantic, 7% in the Brazil–Malvinas confluence, 27% in the eastern equatorial Atlantic, 13% in the Angola Front, and 52% in the Agulhas Leakage (inner triangles in Fig. 7a). This is in stark contrast with the

average for all years between 1999 and 2018 of no more than 3% of the total area for all six regions (Fig. 7b).

El Niño events have a strong impact on the atmospheric circulation of the tropical and South Atlantic. Strong El Niño events, such as 2015/16 propagate their signal to the tropical Atlantic via atmospheric

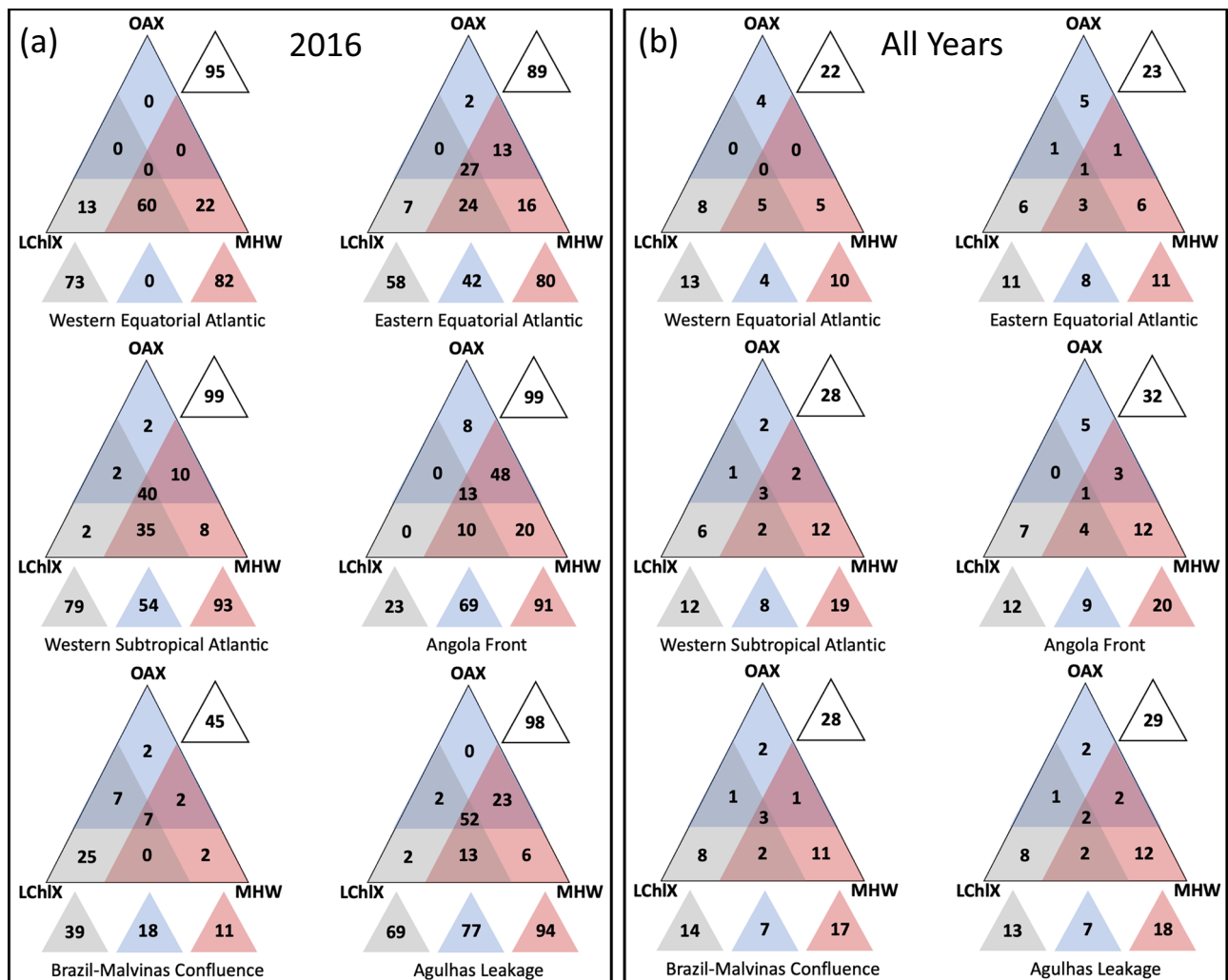


Fig. 7 | The role of El Niño on triple compound events in the South Atlantic. Spatial coverage of compound extreme events in **a** 2016 and **b** averaged over all years for the six selected regions. For each region, rhombuses near the vertices of the larger triangle represent the area covered by a single extreme of marine heat-waves (MHW, red), high acidity (OAX, blue), and low chlorophyll (LChIX, grey). Triangles between the rhombuses represent the area covered by double

compounds of MHW-OAX, OAX-LChIX, and LChIX-MHW. The smaller inner triangle represents the area covered by triple compound events. The outside red triangle represents the area covered by MHW (with or without other extremes), the same for OAX in blue and LChIX in grey. The outside white triangle represents the total area covered by any extreme or combination of extremes.

Kelvin waves⁶⁰, leading to the weakening of trades over the tropical Atlantic. For the mature phase of the 2015/16 El Niño, this is depicted by westward anomalies in Fig. 8a. As a consequence, positive SST anomalies tend to develop in the western equatorial Atlantic via the WES mechanism and in the eastern equatorial Atlantic via Bjerknes feedback, as shown in the last section (Fig. 4c,e). El Niño also affects the South Atlantic via extra-tropical teleconnections by triggering Rossby wave trains^{61,62} (Fig. 8b) that shift the South Atlantic subtropical high poleward (represented by an anticlockwise circulation, H in Fig. 8a), causing warming in the Brazil–Malvinas confluence and Agulhas leakage regions, as discussed in the last section. Moreover, the Rossby wave trains are responsible for the persistent high-pressure system in the western subtropical Atlantic (H in Fig. 8b) that leads to the warming there (Fig. 4d).

Discussion

Ocean extreme events in the equatorial and South Atlantic impact marine life and the livelihood of communities in both South America and Africa. MHWs have become broader, more frequent, and stronger in the equatorial and South Atlantic in recent years, with more pronounced rates of change in the austral summer. In a season where

ocean temperatures are already at their maximum, additional extreme warming can threaten marine species. The stronger warming in the summer, already underway in most of the equatorial and South Atlantic, is expected to persist in the coming century as the SST seasonality increases due to enhanced ocean stratification⁶³.

The consequences of more powerful MHWs can be amplified by the combination with other extreme events, such as extremes of OAX and LChIX. In the equatorial and South Atlantic, the frequency and intensity of these compound events have increased dramatically over the past two decades, peaking in the most recent years. In all selected regions, they have occurred almost every year since 2014, which may limit the recovery of marine ecosystems from these compound extremes. Our analyses also show that these extreme events are interdependent, and as such, they are indeed compounded. Ocean warming combined with acidification can negatively affect many species' survival, growth, and development^{64,65} and shifts in community structure⁶⁶. There is evidence that, for the California current System, this can be mitigated by an increase in food availability⁶⁷. However, our study shows that in the equatorial and South Atlantic, double compound extremes of MHW and OAX often co-occur with LChIX concentrations and, therefore, a decrease in production at the base of the

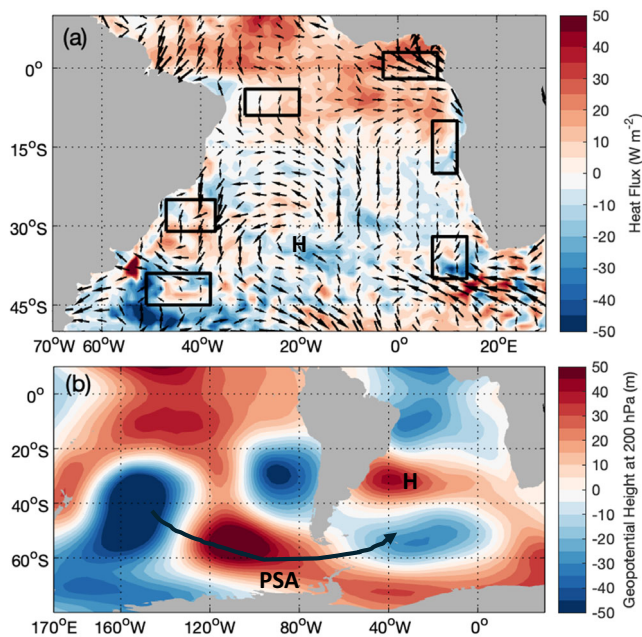


Fig. 8 | El Niño as the primary remote driver of triple compound events.

a Monthly anomalies of surface heat flux (shades, W/m^2) and surface wind (vectors, m/s) during the mature phase of El Niño from December 2015 to February 2016. Positive anomalies of surface heat flux indicate anomalous flux from the atmosphere to the ocean. Black boxes show the six selected regions. **b** Anomalies of geopotential height at 200 hPa (m) for the same period, depicting the Rossby wave trains triggered by El Niño, known as the Pacific-South America (PSA) pattern. In both panels, H indicates the position of the high-pressure system discussed in the text, which is associated with anticyclonic circulation (anticlockwise in the Southern Hemisphere).

food chain. It has been shown recently that the most influential predictor of low-fish biomass events is extremely low net primary production, especially in the subtropics and the mid-latitudes²⁶.

Here, we show that triple compound events are generated by air–sea interaction in the western equatorial Atlantic and western subtropical Atlantic via the WES mechanism and atmospheric blocking, respectively. Weakening of upwelling in the eastern equatorial Atlantic can cause triple compound events via Bjerknes feedback. Triple compound events are associated with poleward shifts of fronts in the Angola Front and Brazil–Malvinas confluence regions, while eddy trapping enhances the occurrence of triple compound events in the Agulhas leakage region. Although our analyses do not show the causal relationship between MHWs and extremes of OAX and LChIX concentration due to the data limitation, the local drivers described here are likely the dominant mechanisms when the three extreme events occur simultaneously. In other words, the three extremes have a common driver described for each region, but this does not imply that the warming (MHW) leads to the LChIX or OAX. For instance, for the confluence region, Brazil current can advect warm, nutrient-poor and high acidity waters, while in the western subtropical South Atlantic, the warming is most likely causing the reduction in nutrients (and chlorophyll concentration) and increase in acidity. In addition, to prove the causal relationship, we would have to have daily data for all three extremes, which are not available, to evaluate the temporal evolution of specific cases.

Past studies have shown that ENSO is one of the significant drivers of MHW globally^{10,28}. Here, we show that in the equatorial and South Atlantic, the strong El Niño event in 2015/16 was responsible for generating the triple compound events. The teleconnections from the tropical Pacific weakened the southeasterly trade winds that caused the triple compound events in the equatorial Atlantic and Angola Front

during austral summer. The southward shift of the South Atlantic subtropical high on the eastern side of the basin caused the triple compound event in the Agulhas Leakage. This shift of the subtropical high combined with a persistent anticyclonic circulation over the western side of the subtropical South Atlantic is responsible for the triple compound extreme in the western subtropical South Atlantic and Brazil–Malvinas confluence regions.

In this study, we use a fixed baseline because this approach reflects the increasingly frequent and devastating biological impacts of compound extreme events⁶⁸. Also, our understanding is that a shifting baseline approach is more appropriate when long periods are considered, such as in climate projection studies⁶⁹. This differs from our case, given the short period analysed here. Moreover, identifying a trend in two decades is uncertain, which may result in artefacts in the identified extremes. Finally, our study shows that marine ecosystems have been exposed to higher SST and $[\text{H}^+]$ and lower chlorophyll levels in the equatorial and South Atlantic during the last two decades.

These ocean extremes impact marine ecosystems, food availability, and thus, local and global economies⁷. As growing ocean extremes pose increasing challenges to coastal areas, climate adaptation and improving coastal resilience should be key objectives in planning and implementing coastal zone policies. Successful adaptation draws on a wide range of information sources, including modelling. In particular, next-generation climate and weather models can provide the unprecedented ability to forecast these events⁷⁰. The fact that triple compound events are widespread over the equatorial and South Atlantic during an El Niño event is important because MHWs can be skilfully predicted mainly due to ENSO⁷⁰. If the forecasts are initialised during an El Niño or La Niña event, MHW forecast skill is enhanced in many regions⁷⁰, particularly in the equatorial and South Atlantic (see their Fig. 3). Thus, the results presented here suggest that improving models' performance in simulating ENSO can help to develop better early warning systems that in turn can be integrated into disaster preparedness and long-term adaptation. Solutions that adapt to climate change can yield multiple co-benefits, including safeguarding marine food production and other ecosystem services and supporting progress toward achieving the UN sustainable development goals.

Methods

Defining the extremes and data sets

The daily $0.25^\circ \times 0.25^\circ$ SST for the period 1982–2020 are obtained from the NOAA optimum interpolation SST (OISST) dataset, which combines in situ and satellite observations^{71,72}. Following the standard methodology², an MHW event is defined when the SST is above the 90th percentile of a seasonally varying climatology for at least five consecutive days. Long-term trends are calculated using a linear least-squares fit from 1982 to 2020, and the nonparametric test of Mann–Kendall is used to assess their significance at the 95% confidence level.

The daily total mixed layer chlorophyll concentration ($[\text{Chl}]$) for the period 1998–2018 is obtained from the NASA Ocean Biogeochemical Model (NOBM.R2020.1 version) dataset with spatial resolutions of 1.25° in longitude by 0.67° in latitude⁷³. Since daily $[\text{Chl}]$ observations from satellites are sparse and limited by cloud cover, this product assimilates satellite observations of $[\text{Chl}]$ from the sea-viewing wide field-of-view sensor, the moderate resolution imaging spectro-radiometer Aqua, and the visible infrared imaging radiometer suite. The extreme events of low $[\text{Chl}]$ are calculated as those in which the daily $[\text{Chl}]$ is below the 10th percentile of a seasonally varying climatology for the period 1998–2018¹⁷. For simplicity, we refer to extremes of low $[\text{Chl}]$ as extreme LChIX events throughout the article.

The observation-based monthly surface hydrogen ion concentration ($[\text{H}^+]$) is available at a horizontal resolution of $1^\circ \times 1^\circ$ for the period 1982–2021. It is derived from the monthly fields of temperature,

salinity (both Hadley Centre EN4.2.2 objective analyses⁷⁴), fugacity of CO₂ (fCO₂) (MPI-SOMFNN v2022^{75–77}) and total alkalinity (LIARv2 algorithm⁷⁸) as described in detail in^{19,23}. The extreme events of high [H⁺] are defined as those months in which [H⁺] is above the 90th percentile of the monthly climatology²³. Note that the skill of the observation-based [H⁺] data in representing responses in [H⁺] during extreme events depends on the underlying neural network-interpolated data for the fCO₂. Due to relatively few fCO₂ measurements in the South Atlantic⁷⁷, these data are comparably uncertain in this region, particularly in the eastern and southern parts of the basin. Future efforts should increase the number of fCO₂ measurements in these regions. Again, for simplicity, we refer to extremes of high [H⁺] as extreme high-acidity (OAX) events, as used in refs. 19,23.

Defining compound extremes

Before calculating the compound extreme events, extreme event intensities are calculated as the anomalies for each extreme event in relation to their climatology. Since the acidity dataset is monthly, the daily MHW and LChIX intensities are combined into monthly cumulative intensities, representing the sum of all daily intensities in each month. The monthly cumulative intensities are then interpolated to have the same spatial resolution of 1° of latitude by 1.25° of longitude. An extreme month of OAX is then considered when the monthly cumulative intensities pass the 90th percentile, and for the monthly cumulative intensities of other extremes, we use a threshold of the 50th percentile. Overall, using the 50, 60, and 70th percentiles for the latter yielded similar spatial patterns, confirming the robustness of the results. The three datasets overlap for the period of 1998–2018. However, since our analyses of compound events involve a comparison of frequencies between two periods, we decided to use periods of the same length (10 years each). Thus, we present our results for 1999–2018. Throughout this article, the term “triple compound events” refers to those multivariate extreme events⁷⁹ of MHW, OAX, and LChIX that co-occur in space and time (Fig. 2, S2 and S3). Similarly, “double compound events” refer to compound events of co-occurring MHW and OAX or MHW and LChIX. To generate the time series of compound extremes for each selected region (Fig. 3), we count months with at least 1% of the area with triple compound events so that it is possible to have every month in the record with extremes. At each grid point, however, extreme values can only occur 10% of the time, considering the thresholds used here (10th and 90th percentiles). The intensity of the triple compound events is the cumulative intensities of MHW, OAX and LChIX averaged within the region for each month and then divided by their standard deviations. For each month, we also calculate the area (%) where the three extreme events overlap within each region (asterisks in Fig. 3).

Defining the selected regions

The six regions are selected based on a qualitative analysis of the occurrence of individual, double and triple compounds in dynamically diverse regions (Figs. 1–2, S1–S3): 1) western equatorial Atlantic between 20–31°W and 4–9°S; 2) western subtropical Atlantic between 37–47°W and 25–31°S; 3) Brazil–Malvinas confluence region between 38–51°W and 39–45°S; 4) eastern equatorial Atlantic between 3°W–8°E and 3°N–2°S; 5) Angola Front between 7–12°E and 10–20°S; 6) Agulhas Leakage between 7–14°E and 32–40°S. In some cases, these areas are biologically productive, such as the eastern equatorial Atlantic, Angola Front, Agulhas Leakage, and Brazil–Malvinas confluence regions. Note, however, that most of the productivity occurs over the continental shelf. Nonetheless, they are still dynamically and biologically important. The domains are depicted by the boxes in Figs. 1 and 2.

Defining the drivers and statistical analysis

To investigate the local and remote drivers of the triple compound events, surface heat fluxes, surface wind, and cloud cover were

obtained from the ECMWF Reanalysis 5th (ERA5) dataset⁸⁰. Mixed-layer depth, thermocline depth and surface ocean velocity were obtained from the Ocean Reanalysis System 5 (ORAS5) dataset⁸¹. The anomaly fields were calculated relative to seasonal climatology for the available period. The composites consist of the differences between the summer months (DJF) with triple compound events and those without triple compound events for 1999–2018. Only statistically significant differences are displayed, using the 95% confidence level given by a standard two-tailed t-test. For the western equatorial Atlantic, we use autumn months (March–April–May (MAM)) because the maximum temperatures occur during this season in this region. The position of Brazil–Malvinas Confluence was calculated as the location of the maximum SST gradient along the 1000-m isobath between 34°S and 41°S, adapting the methodology described by ref. 46. The position of the Angola–Benguela frontal zone was calculated as the location of the maximum SST gradient along the 10°E meridian following the methodology by ref. 50. The SST data used to calculate the fronts were obtained from the OISST product described above. Daily sea surface height data from the Global Ocean Gridded SSALTO/DUACS L4 product with 1/4° of horizontal resolution are used to detect anticyclonic and cyclonic eddies for the period 1998–2018. We apply the Angular Momentum Eddy Detection and Tracking Algorithm (AMEDA)⁸² to identify the number of eddies, the percentage of the area covered by eddies, and their azimuthal speed.

Defining the LMF

The LMF quantifies the dependence between two extreme events when they occur together. It is defined as the ratio of the observed joint probability of the two events to the joint probability assuming independence^{83,84}. When events are independent, the joint probability is $P(A \cap B) = P(A) \times P(B)$. Therefore, the LMF is defined as:

$$LMF = \frac{P(A \cap B)}{P(A) \times P(B)} \quad (1)$$

- If $LMF > 1$, the co-occurrence of A and B is more likely than if they were independent, indicating a positive correlation between the events.
- If $LMF < 1$, it suggests a dampening effect, where the events are less likely to occur together than independently, indicating a negative correlation.
- If $LMF = 1$, it implies that the events are independent.

The LMF was computed for each pair of compound events (MHW–LChIX, MHW–OAX, and OAX–LChIX) according to Eq. (1) using the observed frequencies of the individual events and the observed frequency of their combined occurrence for the period of 1998–2009. The LMF in this study can range from 0 to the upper limit defined by percentile thresholds, which in this case is 10, as the 90th percentile is used as the threshold in the definition of extreme events.

Data availability

The observed daily sea surface temperatures is available from <https://psl.noaa.gov/data/gridded/data.noaa.oisst.v2.highres.html>. The observed daily total mixed layer chlorophyll concentration data are available from https://disc.gsfc.nasa.gov/datasets/NOBM_DAY_R2017/summary. The observation-based monthly surface hydrogen ion concentration data have been deposited in the Zenodo repository under <https://zenodo.org/records/8273342>. The atmospheric reanalysis dataset ERA5 is available from <https://www.ecmwf.int/en/forecasts/dataset/ecmwf-reanalysis-v5> and the ocean reanalysis ORAS5 from <https://www.ecmwf.int/en/forecasts/dataset/ocean-reanalysis-system-5>. Daily sea surface height data are available from https://data.marine.copernicus.eu/product/SEALEVEL_GLO_PHY_L4_NRT_008_046/description.

Code availability

All observational analyses are deposited in Zenodo and can be accessed at <https://doi.org/10.5281/zenodo.14931737>.

References

- Pearce, A. & Feng, M. The rise and fall of the “marine heat wave” off Western Australia during the summer of 2010/2011. *J. Mar. Syst.* **111**, 139–156 (2013).
- Hobday, A. J. et al. A hierarchical approach to defining marine heatwaves. *Prog. Oceanogr.* **141**, 227–238 (2016).
- Cheung, W. & Frolicher, T. Marine heatwaves exacerbate climate change impacts for fisheries in the northeast Pacific. *Sci. Rep.* **10**, 6678 (2020).
- Hughes, T. et al. Global warming transforms coral reef assemblages. *Nature* **556**, 492–496 (2018).
- Smale, D. et al. Marine heatwaves threaten global biodiversity and the provision of ecosystem services. *Nat. Clim. Chang.* **9**, 306–312 (2019).
- Smith, K. et al. Biological impacts of marine heatwaves. *Annu. Rev. Mar. Sci.* **15**, 119–145 (2023).
- Smith, K. et al. Socioeconomic impacts of marine heatwaves: global issues and opportunities. *Science* **374**, eabj3593 (2021).
- Cheung, W. et al. Marine high temperature extremes amplify the impacts of climate change on fish and fisheries. *Sci. Adv.* **7**, eabh0895 (2021).
- Frölicher, T. L., Fischer, E. M. & Gruber, N. Marine heatwaves under global warming. *Nature* **560**, 360–364 (2018).
- Oliver, E. et al. Longer and more frequent marine heatwaves over the past century. *Nat. Commun.* **9**, 1324 (2018).
- Laufkötter, C. et al. High-impact marine heatwaves attributable to human-induced global warming. *Science* **369**, 1621–1625 (2020).
- Oliver, E. Mean warming not variability drives marine heatwave trends. *Clim. Dyn.* **53**, 1653–1659 (2019).
- Costa, N. & Rodrigues, R. R. Future summer marine heatwaves in the western South Atlantic. *Geophys. Res. Lett.* **48**, e2021GL094509 (2021).
- Cael, B. B. et al. Historical and future maximum sea surface temperatures. *Sci. Adv.* **10**, ead5569 (2024).
- Boyd, P. & Brown, C. Modes of interactions between environmental drivers and marine biota. *Front. Mar. Sci.* **2**, 9 (2015).
- Moore, K. et al. Sustained climate warming drives declining marine biological productivity. *Science* **359**, 1139–1143 (2018).
- Le Grix, N., Zscheischler, J., Laufkötter, C., Rousseaux, C. S. & Frölicher, T. L. Compound high-temperature and low-chlorophyll extremes in the ocean over the satellite period. *Biogeosciences* **18**, 2119–2137 (2021).
- Shi, H. et al. Global decline in ocean memory over the 21st century. *Sci. Adv.* **8**, eabm3468 (2022).
- Burger, F., John, J. & Frölicher, T. Increase in ocean acidity variability and extremes under increasing atmospheric CO₂. *Biogeosciences* **17**, 4633–4662 (2020).
- Doney, S. et al. The impacts of ocean acidification on marine ecosystems and reliant human communities. *Annu. Rev. Environ. Resour.* **45**, 83–112 (2020).
- Zeebe, R. E. & Wolf-Gladrow, D. *CO₂ in Seawater: Equilibrium, Kinetics, Isotopes* (Elsevier, 2001).
- Weiss, R. F. Carbon dioxide in water and seawater: the solubility of a non-ideal gas. *Mar. Chem.* **2**, 203–215 (1974).
- Burger, F. A., Terhaar, J. & Frölicher, T. L. Compound marine heatwaves and ocean acidity extremes. *Nat. Commun.* **13**, 4722 (2022).
- Cavole, L. M. et al. Biological impacts of the 2013–2015 warm-water anomaly in the Northeast Pacific: winners, losers, and the future. *Oceanography* **29**, 273–285 (2016).
- Gruber, N. et al. Biogeochemical extremes and compound events in the ocean. *Nature* **600**, 395–407 (2021).
- Le Grix, N. et al. Extreme and compound ocean events are key drivers of projected low pelagic fish biomass. *Glob. Chang. Biol.* **29**, 6478–6492 (2023).
- Holbrook, N. J. et al. Keeping pace with marine heatwaves. *Nat. Rev. Earth Environ.* **1**, 482–493 (2020).
- Holbrook, N. J. et al. A global assessment of marine heatwaves and their drivers. *Nat. Commun.* **10**, 2624 (2019).
- Oliver, E. C. et al. Marine heatwaves. *Annu. Rev. Mar. Sci.* **13**, 313–342 (2021).
- Vogt, L. et al. Local drivers of marine heatwaves: a global analysis with an Earth system model. *Front. Clim.* **4**, 847995 (2022).
- Bian, C. Oceanic mesoscale eddies as crucial drivers of global marine heatwaves. *Nat. Commun.* **14**, 2970 (2023).
- Sen Gupta, A. et al. Drivers and impacts of the most extreme marine heatwave events. *Sci. Rep.* **10**, 1–15 (2020).
- Sarnocchia, S. et al. The anomalous warming of summer 2003 in the surface layer of the Central Ligurian Sea (Western Mediterranean). *Ann. Geophys.* **24**, 443–452 (2006).
- Chen, K., Gawarkiewicz, G. G., Lentz, S. J. & Bane, J. M. Diagnosing the warming of the Northeastern US Coastal Ocean in 2012: a linkage between the atmospheric jet stream variability and ocean response. *J. Geophys. Res. Oceans* **119**, 218–227 (2014).
- Rodrigues, R. R. et al. Common cause for severe droughts in South America and marine heatwaves in the South Atlantic. *Nat. Geosci.* **12**, 620–626 (2019).
- Echevin et al. Forcings and evolution of the 2017 Coastal El Niño Off Northern Peru and Ecuador. *Front. Mar. Sci.* **5**, 367 (2018).
- Di Lorenzo, E. & Mantua, N. Multi-year persistence of the 2014/15 North Pacific marine heatwave. *Nat. Clim. Change* **6**, 1042–1048 (2016).
- Manta, G. et al. The 2017 record marine heatwave in the south-western Atlantic shelf. *Geophys. Res. Lett.* **45**, 12449–12456 (2018).
- Brauko, K. M. et al. Marine heatwaves, sewage and eutrophication combine to trigger deoxygenation and biodiversity loss: a SW Atlantic case study. *Front. Mar. Sci.* **7**, 590258 (2020).
- FAO. The State of World Fisheries and Aquaculture 2018—Meeting the sustainable development goals. Rome. Licence: CC BY-NC-SA 3.0 IGO (2018).
- Pinsky, M. L., Eikeset, A. M., McCauley, D. J., Payne, J. L. & Sunday, J. M. Greater vulnerability to warming of marine versus terrestrial ectotherms. *Nature* **569**, 108–111 (2019).
- Xie, S. & Philander, S. G. A coupled ocean-atmosphere model of relevance to the ITCZ in the eastern Pacific. *Tellus A Dyn. Meteorol. Oceanogr.* **46**, 340–350 (1994).
- Chang, P., Fang, Y., Saravanan, R., Ji, L. & Seidel, H. The cause of the fragile relationship between the Pacific El Niño and the Atlantic Niño. *Nature* **443**, 324–328 (2006).
- Keenlyside, N. & Latif, M. Understanding equatorial Atlantic interannual variability. *J. Clim.* **20**, 131–142 (2007).
- Okumura, Y. & Xie, S. P. Some overlooked features of tropical Atlantic climate leading to a new Niño-like phenomenon. *J. Clim.* **19**, 5859–5874 (2006).
- Goni, G. J., Bringas, F. and DiNezio, P. N. Observed low-frequency variability of the Brazil Current front. *J. Geophys. Res. Oceans* **116**, 7198 (2011).
- Rouault, M., Illig, S., Lübbecke, J. & Koungue, R. A. I. Origin, development and demise of the 2010–2011 Benguela Niño. *J. Mar. Syst.* **188**, 39–48 (2018).
- Bachèlery, M. L., Illig, S. & Dadou, I. Interannual variability in the South-East Atlantic Ocean, focusing on the Benguela upwelling system: remote versus local forcing. *J. Geophys. Res. Oceans* **121**, 284–310 (2016).
- Bachèlery, M. L., Illig, S. & Dadou, I. Forcings of nutrient, oxygen, and primary production interannual variability in the southeast Atlantic Ocean. *Geophys. Res. Lett.* **43**, 8617–8625 (2016).

50. Vizy, E. K., Cook, K. H. & Sun, X. Decadal change of the South Atlantic Ocean Angola–Benguela frontal zone since 1980. *Clim. Dyn.* **51**, 3251–3273 (2018).
51. Ford, D. J. et al. Mesoscale eddies enhance the air-sea CO₂ sink in the South Atlantic Ocean. *Geophys. Res. Lett.* **50**, 2137 (2023).
52. Orselli, I. et al. The sea-air CO₂ net fluxes in the South Atlantic Ocean and the role played by Agulhas eddies. *Prog. Oceanogr.* **170**, 40–52 (2019).
53. Woosley, R. J., Millero, F. J. & Wanninkhof, R. Rapid anthropogenic changes in CO₂ and pH in the Atlantic Ocean: 2003–2014. *Glob. Biogeochem. Cycles* **30**, 70–90 (2016).
54. Song, H. et al. Mesoscale modulation of air-sea CO₂ flux in Drake Passage. *J. Geophys. Res. Oceans* **121**, 6635–6649 (2016).
55. Knutson, T. R. et al. CMIP5 model-based assessment of anthropogenic influence on record global warmth during 2016, [in “Explaining Extreme Events of 2016 from a Climate Perspective”]. *Bull. Am. Meteorol. Soc.* **99**, S11–S15 (2018).
56. Santoso, A., McPhaden, M. J. & Cai, W. The defining characteristics of ENSO extremes and the strong 2015/2016 El Niño. *Rev. Geophys.* **55**, 1079–1129 (2017).
57. World Health Organization. El Niño affects more than 60 million people. Available in <https://www.who.int/news-room/feature-stories/detail/el-niño-affects-more-than-60-million-people>, accessed on 7 June 2022 (2016).
58. Walsh, J. E. et al. The high latitude marine heat wave of 2016 and its impacts on Alaska [in “Explaining Extreme Events of 2016 from a Climate Perspective”]. *Bull. Am. Meteorol. Soc.* **99**, S39–S43 (2018).
59. Imada, Y. et al. Climate change increased the likelihood of the 2016 heat extremes in Asia [in “Explaining Extreme Events of 2016 from a Climate Perspective”]. *Bull. Am. Meteorol. Soc.* **99**, S97–S101 (2018).
60. Chiang, J. C. & Sobel, A. H. Tropical tropospheric temperature variations caused by ENSO and their influence on the remote tropical climate. *J. Clim.* **15**, 2616–2631 (2002).
61. Rodrigues, R. et al. The impacts of Inter-El Niño variability on the tropical Atlantic and northeast Brazil climate. *J. Clim.* **24**, 3402–3422 (2011).
62. Rodrigues, R., Campos, E. & Haarsma, R. The Impact of ENSO on the South Atlantic subtropical dipole mode. *J. Clim.* **28**, 2691–2705 (2015).
63. Jo, A. R. et al. Future amplification of sea surface temperature seasonality due to enhanced ocean stratification. *Geophys. Res. Lett.* **49**, e98607 (2022).
64. Harvey, B. P., Gwynn-Jones, D. & Moore, P. J. Meta-analysis reveals complex marine biological responses to the interactive effects of ocean acidification and warming. *Ecol. Evol.* **3**, 1016–1030 (2013).
65. Kroeker, K. J. et al. Impacts of ocean acidification on marine organisms: quantifying sensitivities and interaction with warming. *Glob. Change Biol.* **19**, 1884–1896 (2013).
66. Goldenberg, S. U., Nagelkerken, I., Ferreira, C. M., Ullah, H. & Connell, S. D. Boosted food web productivity through ocean acidification collapses under warming. *Glob. Change Biol.* **23**, 4177–4184 (2017).
67. Bednaršek et al. El Niño-related thermal stress coupled with upwelling-related ocean acidification negatively impacts cellular to population-level responses in pteropods along the California current system with implications for increased bioenergetic costs. *Front. Mar. Sci.* **5**, 1–17 (2018).
68. Sen Gupta, A. Marine heatwaves: definition duel heats up. *Nature* **617**, 465–465 (2023).
69. Amaya, D. J., and Coauthors. Marine heatwaves need clear definitions so coastal communities can adapt. *Nature* **616**, 29–32 (2023).
70. Jacox, M. G. et al. Global seasonal forecasts of marine heatwaves. *Nature* **604**, 486–490 (2022).
71. Reynolds et al. Daily high-resolution-blended analyses for sea surface temperature. *J. Clim.* **20**, 5473–5496 (2007).
72. Huang et al. Improvements of the daily optimum interpolation sea surface temperature Version 2.1. *J. Clim.* **34**, 2923–2939 (2021).
73. Gregg, W. and Rousseaux, C. (Eds.): *NASA Ocean Biogeochemical Model Assimilating Satellite Chlorophyll Data Global Daily VR2017* (Goddard Earth Sciences Data and Information Services Center GES DISC, 2017).
74. Good, S. A., Martin, M. J. & Rayner, N. A. EN4: Quality controlled ocean temperature and salinity profiles and monthly objective analyses with uncertainty estimates. *J. Geophys. Res. Oceans* **118**, 6704–6716 (2013).
75. Landschützer, P., Gruber, N. & Bakker, D. C. E. Decadal variations and trends of the global ocean carbon sink. *Glob. Biogeochem. Cycles* **30**, 1396–1417 (2016).
76. Landschützer, P., Gruber, N. & Bakker, D. C. E. An observation-based global monthly gridded sea surface pCO₂ product from 1982 onward and its monthly climatology (NCEI Accession 0160558) (2020).
77. Bakker, D. C. E. and Co-authors. Surface Ocean CO₂ Atlas (SOCAT) V4. PANGAEA. <https://doi.org/10.1594/PANGAEA.866856> (2016).
78. Carter, B. R. et al. Updated methods for global locally interpolated estimation of alkalinity, pH, and nitrate. *Limnol. Oceanogr. Methods* **16**, 119–131 (2018).
79. Zscheischler, J. et al. A typology of compound weather and climate events. *Nat. Rev. Earth Environ.* **1**, 333–347 (2020).
80. Hersbach, H. et al. The ERA5 global reanalysis. *Q. J. R. Meteorol. Soc.* **146**, 1999–2049 (2020).
81. Zuo et al. OCEAN5: The ECMWF Ocean Reanalysis System and Its Real-time Analysis Component. *Series: ECMWF Technical Memoranda* (2018).
82. Le Vu, B., Stegner, A. & Arsouze, T. Angular momentum eddy detection and tracking algorithm (AMEDA) and its application to coastal eddy formation. *J. Atmos. Ocean. Technol.* **35**, 739–762 (2018).
83. Zscheischler, J. & Seneviratne, S. I. Dependence of drivers affects risks associated with compound events. *Sci. Adv.* **3**, e1700263 (2017).
84. Ridder, N. N. et al. Global hotspots for the occurrence of compound events. *Nat. Commun.* **11**, 5956 (2020).

Acknowledgements

This study was supported by the TRIATLAS project funded under the European Union’s Horizon 2020 Programme (Grant Agreement #817578; R.R.R., A.G.N., N.K., P.S.B., J.M.A.), by the National Ocean Observation and Monitoring Network (ReNOMO) project funded by the National Council for Scientific and Technological Development (CNPq, Grant Agreement #409666/2022), and is part of PPGOceano-UFSC. T.L.F. and F.A.B. were supported by the Bloom Foundation of the University of Bern.

Author contributions

The initial study was designed by R.R.R. and A.G.N. The analyses were conducted by R.R.R., A.G.N., C.A., P.S.B. and J.A. R.R.R., C.A., A.G.N., T.L.F., N.K., A.J.H., F.A.B., P.S.B. and J.A. contributed ideas and discussed results. R.R.R. wrote the initial draft and C.A., A.G.N., T.L.F., N.K., A.J.H., F.A.B., P.S.B., J.A. contributed to the writing.

Competing interests

The authors declare no competing interests.

Additional information

Supplementary information The online version contains supplementary material available at <https://doi.org/10.1038/s41467-025-58238-y>.

Correspondence and requests for materials should be addressed to Regina R. Rodrigues.

Peer review information *Nature Communications* thanks Weiwei Fu, Changyu Li, and the other, anonymous, reviewer for their contribution to the peer review of this work. A peer review file is available.

Reprints and permissions information is available at <http://www.nature.com/reprints>

Publisher's note Springer Nature remains neutral with regard to jurisdictional claims in published maps and institutional affiliations.

Open Access This article is licensed under a Creative Commons Attribution-NonCommercial-NoDerivatives 4.0 International License, which permits any non-commercial use, sharing, distribution and reproduction in any medium or format, as long as you give appropriate credit to the original author(s) and the source, provide a link to the Creative Commons licence, and indicate if you modified the licensed material. You do not have permission under this licence to share adapted material derived from this article or parts of it. The images or other third party material in this article are included in the article's Creative Commons licence, unless indicated otherwise in a credit line to the material. If material is not included in the article's Creative Commons licence and your intended use is not permitted by statutory regulation or exceeds the permitted use, you will need to obtain permission directly from the copyright holder. To view a copy of this licence, visit <http://creativecommons.org/licenses/by-nc-nd/4.0/>.

© The Author(s) 2025